THE ATMOSPHERIC 60-GHz OXYGEN SPECTRUM: Modeling and Laboratory Measurements

Hans J. Liebe, George A. Hufford, and Robert O. DeBolt*

Molecular oxygen dominates the attenuation and delay rates of dry air throughout the V-band (50-75 GHz). Both rates display as a function of altitude an intricate pattern which, for the most part, has never been confirmed by experiment. The collective spectral behavior of 38 pressure-broadened $\mathbf{O}_2$ lines is described by a complex prediction model (MPM89). For atmospheric conditions of pressure equivalent to altitudes between sea level and 30 km (100 to 1 kPa), this behavior was studied under controlled laboratory conditions. The spectrometer consisted of a one-port Fabry-Perot resonator, which was excited by an automatic network analyzer. All operations were controlled by a microcomputer, including reference level calibrations at multiple (up to 15, separated by 0.73 GHz) resonances and control of the pressure steps. Introducing gas into the spectrometer cell changed the detected resonance response, from which was deduced a complex refractivity by means of a twin, nonlinear least squares method. The analysis of dry air measurements concentrated on the loss part, expressed as attenuation rate α in dB/km. The detection sensitivity was ± 0.01 dB/km for an effective path length of 0.24 km and a 5 percent coupling ratio of a resonance response. Coupling to a particular resonance and the duration (1-5 hrs) of a measurement sequence influenced the spectrometer performance. Over 4,000 attenuation values are reported. The results were measured between 53.9 and 66.3 GHz in 0.1 GHz frequency increments at eleven pressure steps (1-100 kPa) for three temperatures (7,30,52°C). The measurement uncertainties were estimated to be typically ± 0.05 below 3 dB/km and ± 2 percent for higher values (≤ 18 dB/km). A first comparison of experimental results with MPM89 predictions revealed, in addition to random data scatter, systematic differences that correlate with line broadening and overlap parameters.

Key Words: atmospheric oxygen spectrum; dry air; frequency range: 54 to 66 GHz; frequency, pressure and temperature parameters; laboratory attenuation measurements; parametric studies

1. INTRODUCTION

For V-band radio frequencies (50 to 75 GHz), molecular oxygen turns the atmosphere below 90 km altitude into an absorptive and dispersive medium. Accurate modeling of the spectral response is important for predicting the propagation of radiation through the atmosphere. At heights above 12 km where pressures are less than 20 kilopascal (200 mb), there is a definite line spectrum with more than 25 discernable features spread over the 50 to 70 GHz range. At lower heights, the increasing pressure broadens the lines and causes them to blend together. The composite shape resembles a band centered at 60 GHz; however, the resulting intensity is not the simple sum of isolated line responses. Instead, there is an "overlap interference", which is taken into account in a theory developed by Rosenkranz (1988; 1991) by means of pressure-proportional coefficients attached to each line of the $\mathbf{O}_2$ microwave spectrum.

* The authors are with the Institute for Telecommunication Sciences, National Telecommunications and Information Administration,. U.S. Department of Commerce, Boulder, CO 80303.

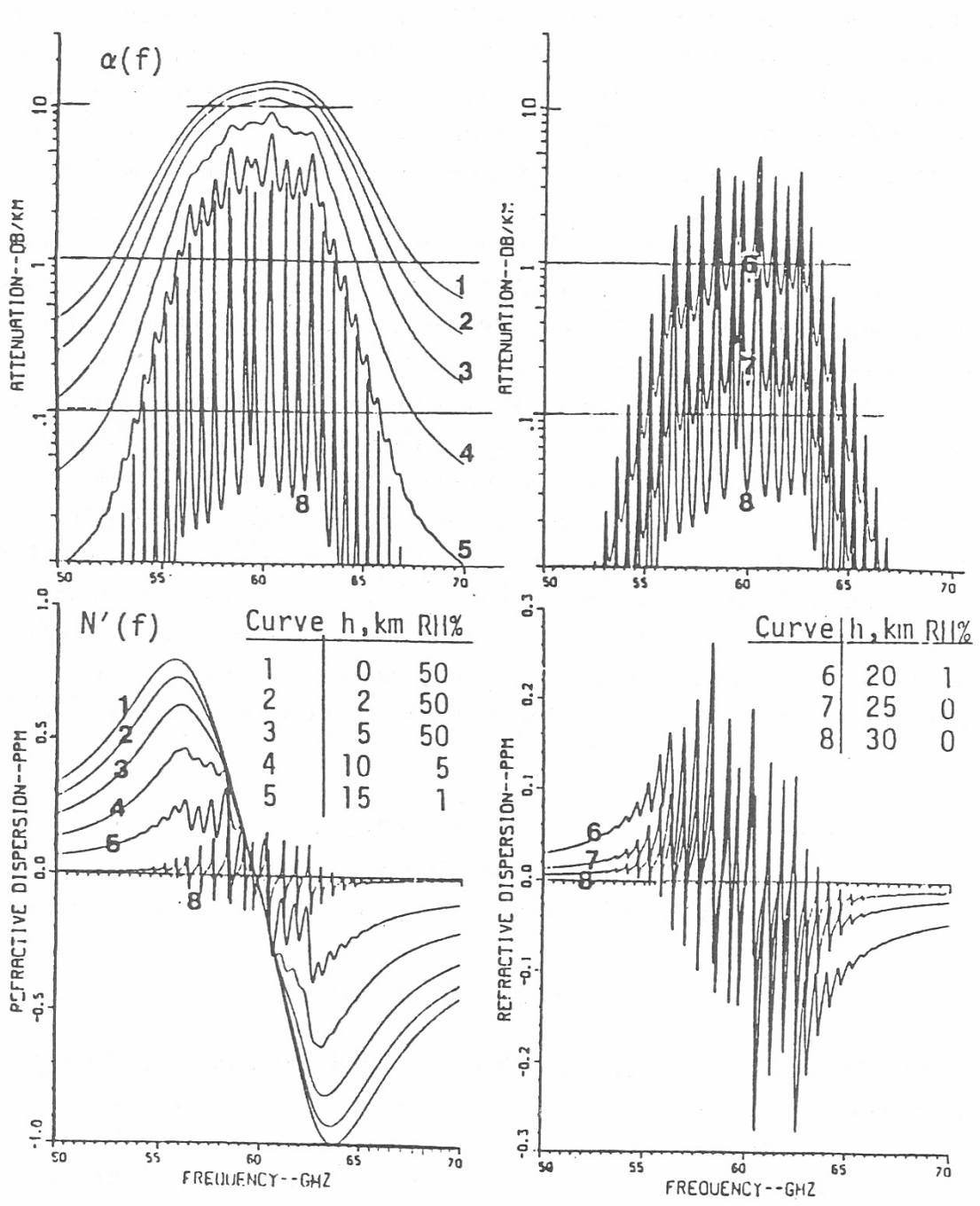

Figure 1. Attenuation rate $\alpha(f)$ and refractivity $N'(f)$ of dry air (O2 spectrum) between 50 and 70 GHz, predicted by MPM89 for simulated conditions (U.S. Std. Atm.) at altitudes, H = 0 to 30 km.

Spectral properties of a gas may be expressed in terms of attenuation rate α in decibels per kilometer (dB/km) and refractivity N′ in parts per million (ppm). Frequency and height (pressure) dependence of these quantities for the atmospheric $\mathbf{O}_2$ spectrum between 50 and 70 GHz are depicted in Figure 1. The graphs encompass various stages from an unstructured band at sea level to isolated line behavior at 30-km height. Model predictions of these highly frequency-selective atmospheric transfer characteristics need to be corroborated by controlled laboratory studies, where frequency, pressure, and temperature provide the variables.

1.1 Overview

The main body of this report deals with the analytical and experimental aspects of the dry air module in the millimeter-wave propagation model MPM89 (Liebe, 1989). The multi-coefficient formulation of the atmospheric $\mathbf{O}_2$ spectrum has been called the Rosenkranz-Liebe model (e.g., Hill, 1987). Details of an experiment are given that provides high quality data for a comparison with model predictions. Precision measurements of the signal reflected from a one-port resonator were used. Interactive spectrometer operations, automatic recordings, and data reduction to attenuation rates α (and refractivities N′) were handled by a microcomputer. Optimization problems of the detection scheme, repeatability problems, and various experimental procedures are described in detail. Factors that influence precision and accuracy of the measurements are examined, examples are given, and the final results are summarily compared with model predictions. Possible corrections to the physical model MPM89 are discussed. In the Appendix, the measured attenuation rates α_x are tabulated and compared with MPM predictions. The extensive database contains information on the interaction process between colliding air molecules. Systematic deviations from model predictions challenge future theoretical efforts.

2. MPM89: A PREDICTION MODEL FOR THE ATMOSPHERIC 60 GHz O_2 SPECTRUM

2.1 Complex Refractivity

For a quantitative description of the $\mathbf{O}_2$ microwave spectrum the measure of complex refractivity,

$$N(f) = N_s + N'(f) - jN''(f) \quad \text{ppm}, \tag{1}$$

is adopted (Liebe, 1989). The nondispersive part N_s is real and positive; the frequency-dependent refractive dispersion and loss contributions are denoted by $N' - jN''$, which for $\mathbf{O}_2$ microwave transitions are represented by the sum of a line (resonant) and a relaxation (nonresonant) term, $N_L + N_D$; the unit ppm denotes 1×10^{-6}; and $j = \sqrt{-1}$. Converted into conventional radio engineering quantities, the imaginary part defines power attenuation α and the real part phase delay β, expressed as

$$\alpha = 0.1820 \cdot f \cdot N''(f) \quad \text{dB/km} \quad \text{and} \quad \beta = 1.2008 \cdot f \cdot N'(f) \quad \text{deg/km}, \tag{2}$$

where the frequency f is GHz. The numerical factors derive from $(4\pi/c)10\log e = 0.1820$; c = 299.792 458 km·GHz·ppm^{-1} is the speed of light in vacuum; and 360/c = 1.2008.

The refractivity **N** is proportional to the number of molecules per unit volume, which is computed from the known quantities of pressure P (kPa) and temperature T (K) assuming the ideal gas law. The nondispersive term of the three gases of interest here is then given by

$$N_s = 792.06 \cdot r_G (P/T) \quad \text{ppm}, \tag{3}$$

where the factor $r_G \equiv r_{N2} = 1.0000(3)$[1] is the experimental value obtained for nitrogen by Newell and Baird (1965). Measurements at 60 GHz assuming $r_{N2} = 1$ (Liebe et al., 1977) yielded :

$r_{Air} = 0.98003(32)$ for CO_2-free, dry air

and

$r_{O2} = 0.9033(22)$ for Oxygen.

2.2 Line Spectrum

Resonance contributions from 44 oxygen lines are calculated by means of a line-by-line summation,

$$N_L = \sum_k S_k \mathbf{F}_k \quad \text{ppm}, \tag{4}$$

where

$$S_k = a_1 P \cdot \theta^3 \exp[a_2(1 - \theta)] \quad \text{kHz}, \tag{5}$$

is a line strength; $\theta = 300/T$ is a relative inverse temperature variable; $\mathbf{F}_k$ is a complex shape function in GHZ^{-1}; k is an index for 38 $\mathbf{O}_2$ fine structure transitions (quantum number code, $K^{\pm} = 1$ to 37) and 6 rotational lines below 1000 GHz; and a_1, a_2 are spectroscopic coefficients (see Table 1).

The shape function of an isolated, pressure-broadened line was formulated by Van Vleck-Weisskopf (e.g., Hill, 1987) and modified by Rosenkranz (1988) to include pressure-induced line interference as follows:

$$F(f) = \frac{f}{\nu_k}\left[\frac{1 + jI_k}{\nu_k - f + j\gamma_k} - \frac{1 - jI_k}{\nu_k + f - j\gamma_k}\right] \tag{6}$$

which may be rationalized to absorption (F″) and dispersion (F′) profiles

[1] Throughout this report, digits in parentheses at the end of a numerical value give its standard deviation in terms of the final listed digits.

$$F''(f) = A(X + Y) - I_k\,[(1 - B)X + (1 + B)Y],$$

and

$$F'(f) = (1 - B)X - (1 + B)Y + I_k \cdot A(X - Y),$$

with the abbreviations

$$A = \gamma_k/\nu_k, \qquad B = f/\nu_k,$$
$$X = f/[(\nu_k - f)^2 + \gamma_k^2], \qquad Y = f/[(\nu_k + f)^2 + \gamma_k^2].$$

Width and interference parameters of (6) are for $\mathbf{O}_2$ lines in air,

$$\gamma_k = a_3 P \cdot \theta^{\eta} \quad \text{GHz}, \tag{7}$$

where $\eta = (0.8 - a_4)$ and

$$I_k = (a_5 + a_6\,\theta) P \cdot \theta^{0.8}. \tag{8}$$

Table 1 lists center frequencies $\nu_k(K^{\pm})$ in GHz (Zink and Mizushima, 1987) for strengths $a_1 \geq 3 \times 10^{-7}$ kHz; and the spectroscopic coefficients a_2, a_5 and a_6 from Rosenkranz (1991) and a_1, a_3 and a_4 (for $f \leq 300$ GHz we have $a_4 = 0$) from Liebe (1989) for strength S_k , pressure-broadened width γ_k and pressure-induced interference I_k , all at $\theta = 1$.

At height levels above 30 km ($P \leq 1$ kPa), the geomagnetic field imposes Zeeman-splitting on the $\mathbf{O}_2$ lines and the refractivity **N** becomes a three-dimensional tensor. As a consequence, radiowave propagation in the vicinity ($\nu_k \pm 5$ MHz) of $\mathbf{O}_2$ line-centers is direction-dependent and polarization-sensitive (Hufford and Liebe, 1989).

2.3 Relaxation Spectrum

The nonresonant refractivity of dry air makes a small contribution at ground level pressures due to the relaxation (Debye) spectrum of oxygen (Liebe, 1985), which is computed with

$$\mathbf{N}_D = S_o \mathbf{F}_o \qquad \text{ppm}, \tag{9}$$

The strength is given by

$$S_o = 6.14 \times 10^{-4} P \cdot \theta^2 \qquad \text{ppm}, \tag{9a}$$

and the complex Debye shape is

Table 1

Line Frequencies And Coefficients For Microwave Transitions Of $\mathbf{O}_2$ In Air

ν_o	a_1	a_2	a_3	$a_4 = 0$	a_5	a_6
GHz	kHz/kPa $\times 10^{-6}$		GHz/kPa $\times 10^{-3}$		1/kPa $\times 10^{-3}$	1/kPa $\times 10^{-3}$
50.474239	0.94	9.694	8.60		1.600	5.520
50.987747	2.46	8.694	8.70		1.400	5.520
51.503349	6.08	7.744	8.90		1.165	5.520
52.021412	14.14	6.844	9.20		0.883	5.520
52.542393	31.02	6.004	9.40		0.579	5.520
53.066906	64.10	5.224	9.70		0.252	5.520
53.595749	124.70	4.484	10.00		–0.066	5.520
54.130001	228.00	3.814	10.20		–0.314	5.520
54.671158	391.80	3.194	10.50		–0.706	5.520
55.221367	631.60	2.624	10.79		–1.151	5.514
55.783802	953.50	2.119	11.10		–0.920	5.025
56.264774	548.90	0.015	16.46		2.881	–0.069
56.363388	1344.00	1.660	11.44		–0.596	4.750
56.968204	1763.00	1.260	11.81		–0.556	4.104
57.612484	2141.00	0.915	12.21		–2.414	3.536
58.323875	2386.00	0.626	12.66		–2.635	2.686
58.446590	1457.00	0.084	14.49		6.848	–0.647
59.164207	2404.00	0.391	13.19		–6.032	1.858
59.590984	2112.00	0.212	13.60		8.266	–1.413
60.306061	2124.00	0.212	13.82		–7.170	0.916
60.434776	2461.00	0.391	12.97		5.664	–2.323
61.150558	2504.00	0.626	12.48		1.731	–3.039
61.800156	2298.00	0.915	12.07		1.738	–3.797
62.411217	1933.00	1.260	11.71		–0.048	–4.277
62.486259	1517.00	0.083	14.68		–4.290	0.238
62.997978	1503.00	1.665	11.39		0.134	–4.860
63.568520	1087.00	2.115	11.08		0.541	–5.079
64.127769	733.50	2.620	10.78		0.814	–5.525
64.678902	463.50	3.195	10.50		0.415	–5.520
65.224068	274.80	3.815	10.20		0.069	–5.520
65.764771	153.00	4.485	10.00		–0.143	–5.520
66.302094	80.09	5.225	9.70		–0.428	–5.520
66.836830	39.46	6.005	9.40		–0.726	–5.520
67.369598	18.32	6.845	9.20		–1.002	–5.520
67.900864	8.01	7.745	8.90		–1.255	–5.520
68.431007	3.30	8.695	8.70		–1.500	–5.520
68.960312	1.28	9.695	8.60		–1.700	–5.520
118.750343	945.00	0.009	16.30		–0.247	0.003

$$F_d = \frac{1}{1 + jZ} - 1 \tag{10}$$

where imaginary (loss) and real (phase) parts are

$$F_o''(f) = Z/(1 + Z_2) \qquad \text{and} \qquad F_o'(f) = - Z^2/(1 + Z^2),$$

with the abbreviation $Z = f/\gamma_o$. The nonresonant width follows from

$$\gamma_o = 5.6\times10^{-3} P\cdot\theta^{1.05} \quad \text{GHz} \tag{11}$$

The width parameter γ_o was deduced from an MPM -based evaluation of atmospheric emission measurements between 2.5 and 10 GHz (Danese and Partridge, 1989).

2.4 Earlier Experimental Studies Between 50 and 75 GHz

The characteristics α(f) and N′(f) of the 60-GHz $\mathbf{O}_2$ spectrum have been measured on a limited scale under controlled laboratory conditions. Pure oxygen and dry air spectra were studied for variations with frequency f, pressure P, and temperature T under "isolated" and "overlapped" line conditions:

Line studies with oxygen furnished data on self-broadened ($\mathbf{O}_2$ + $\mathbf{O}_2$) width and strength parameters (Liebe et al., 1977). Pressure scans (P = 0 to 3 kPa) of differential refractivity, $\Delta N = N'(P)_f - N'(P)_{f/2}$, were done for 21 of the stronger $\mathbf{O}_2$ lines. The profiles ΔN(P) peak at $P = P_r$ to a value ΔN_o when measured at frequencies, $f = \nu_k \pm 15$ MHz. Isolated line parameters of width ($\gamma_k = \Delta\nu/P_r$) and strength ($S_k = \Delta N_o \gamma_k$) were determined from extrapolations to $f = \nu_k$. For these experiments, the geomagnetic field present in the laboratory was eliminated to avoid any Zeeman effect. Examples of measured data for ΔN_o and P_r are shown in Figure 2. Complementary experimental results for foreign-gas-broadened widths ($\mathbf{O}_2$ + N_2, H_2O, ...) were reported in Table 2 of the reference (Liebe, 1985).

Band behavior of overlapped lines is depicted in Figure 3. The data on complex refractivity **N** were measured for dry air between 53.6 and 63.6 GHz at pressures of 53 and 80 kPa and a temperature of 27°C, and in revised form reported by Liebe and Layton (1987). Rosenkranz fitted our data to his overlap theory (1988) and later (1991), based on our 1987 revisions, published the set of interference coefficients I_k which is listed in Table 1. The attenuation rates shown in Figure 4 are from measurements with pure oxygen at pressures of about 2 atm and two temperatures, -13 and 23°C (Read et al., 1988). Some quoted error bounds exceed ten percent. Nevertheless, these results support the correction of overlap interference effects as implemented in MPM89. The $\mathbf{O}_2$ results were scaled by us to represent dry air.

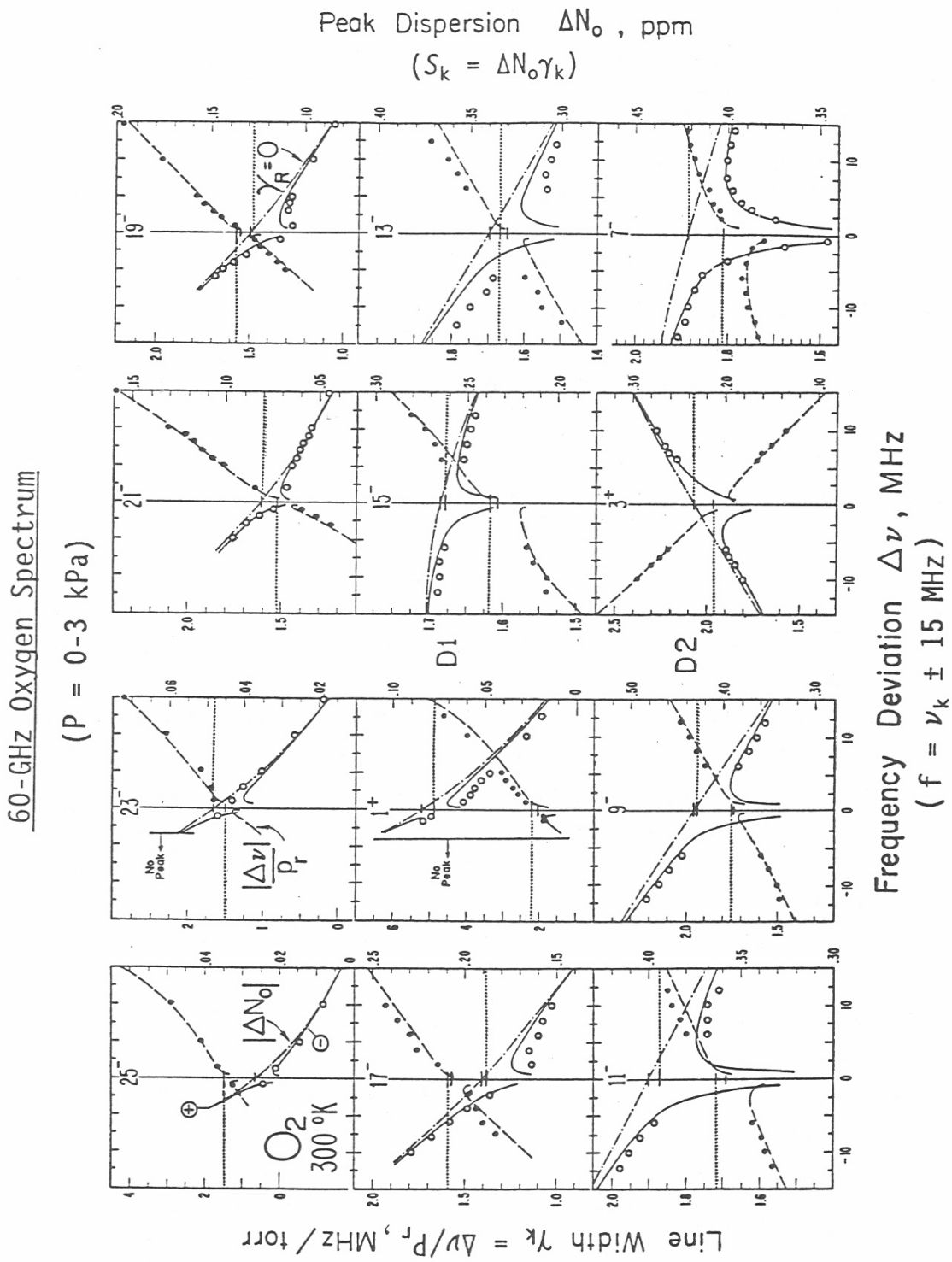

Figure 2. Experimental data on width and peak intensity for twelve pressure-broadened O_2 lines in the 60 GHz range. (for details see Liebe et al., 1977).

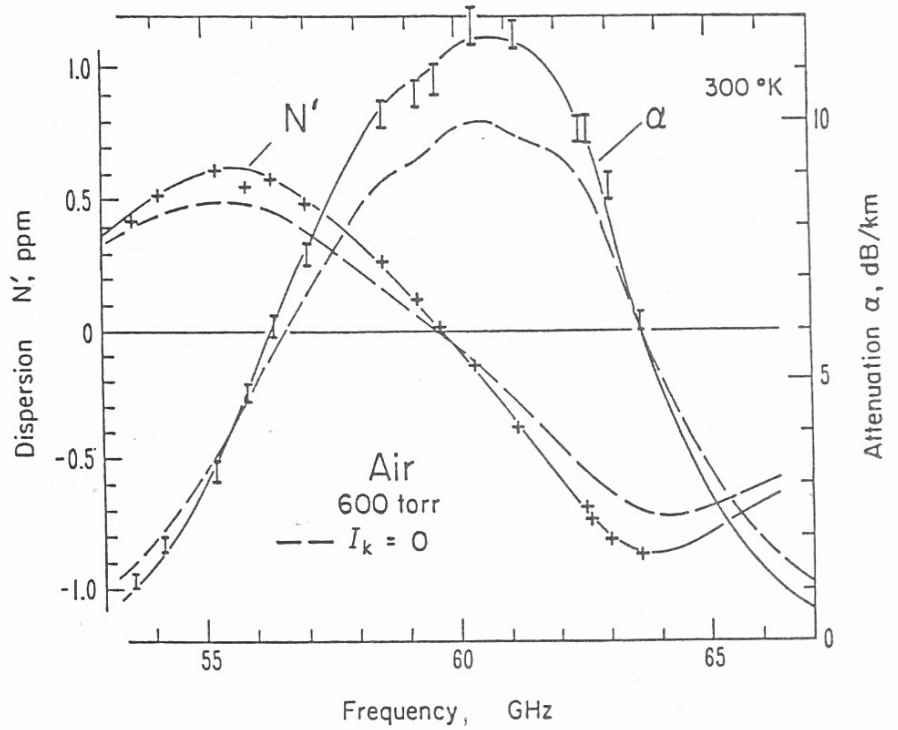

Figure 3. Measured attenuation α and refractivity N′ from 54 to 67 GHz for dry air at 80 kPa (I_k - line interference coefficients).

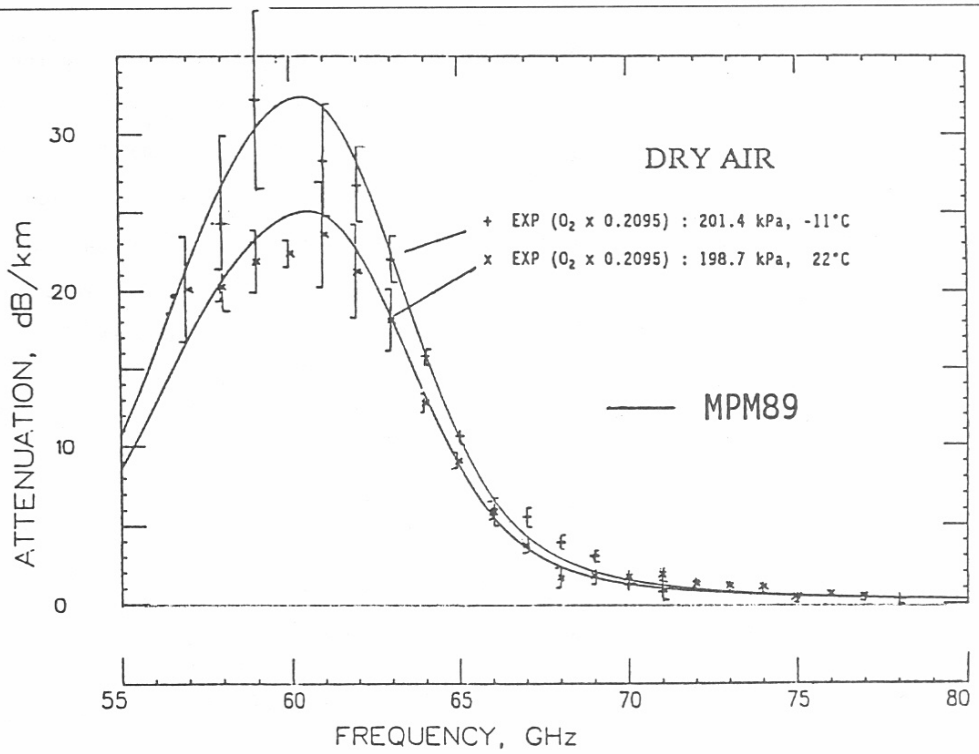

Figure 4. Attenuation data for dry air between 55 and 80 GHz, scaled from measurements of pure O_2 at 200 kPa pressure (Read et al., 1988).

Equations (1) to (11) represent the underlying theory of pressure-broadened, overlapping $\mathbf{O}_2$ lines that describes the spectrum of dry air centered at 60 GHz (Rosenkranz, 1988; 1990). The available range of quantitative data sets suitable to confirm a model for the atmospheric $\mathbf{O}_2$ microwave spectrum is more or less limited to what is shown in Figures 2 through 4. A serious effort to confirm pressure-broadening behavior under quasi-atmospheric conditions has been missing. Laboratory studies of the spectral intensity should focus on temperature and pressure dependences for single-line broadening and multi-line interference effects.

Relevant data are required to test the validity of various theoretical assumptions. Such "truth" data need to have negligible measurement error, must be free of systematic bias, and have to be numerous enough to sample all model dimensions. If we assume that center frequencies ν_k (Zink and Mizushima, 1987) and line strengths $S_k(a_1, a_2)$ (Liebe et al., 1977) are correct, then the values of at least 100 adjustable spectroscopic coefficients (a_3 to a_6, see Table 1) for 25 of the "stronger" lines centered between 54 and 66 GHz have to be determined from fits to measured data. Measurement techniques for such an ambitious undertaking will be discussed next. A comparison of predicted and measured results would check the accuracy of the MPM model and conceivably lead to revisions of the theory which, in turn, would provide an improved understanding of the molecular interaction effects that the theory seeks to describe.

3. THE RESONANCE SPECTROMETER

3.1 Resonator Characteristics

A semiconfocal, one-port Fabry-Perot resonator is the heart of the spectrometer. A flat and a spherical mirror (400 mm radius of curvature; both 100 mm in diameter, silver-plated brass with optically polished surfaces) are separated a distance d_R by three invar rods. The structure is housed in a stainless steel vacuum chamber that is temperature-controlled and can be pressurized (Liebe and Layton, 1987). A cross section of the spectrometer chamber with the resonator can be found in Fig. 2 of Liebe et al. (1984). Resonances were excited via a circular coupling iris centered in the flat mirror, followed by a quartz glass vacuum window, and V-band waveguide. Fundamental TEM_{00q} modes were utilized for which the center frequencies follow from

$$f_x = \frac{c}{n'}\left(\frac{4q-1}{8d_R}\right) \qquad GHz, \tag{12}$$

where c is the speed of light in vacuum, which has in units of mm·GHz the same value given at (2); q is the number of half-wavelength nodes between the mirrors; $n' = 1 + (N_s + N')10^{-6}$ is the real part of the refractive index of the gas inside the resonator, and $d_R = 205 \pm 12$ mm is the mirror spacing, varied with a precision ($\Delta d_R = \pm 0.3$ μm) micrometer. For example, the resonance center for the evacuated cell (P = 0) is at $f_0 = 62.500{,}000$ GHz when q = 85 and $d_R = 204.458{,}456$ mm. The experimental resonance frequency decreases to $f_x = f_0 \cdot [1 - (N_s + N')10^{-6}]$ due to refractive tuning by the gas.

The key parameter of a sensitive spectrometer is its path length. The effective path length of an evacuated, high Q resonator is given by

$$L_E = 23.86/b_0 \quad \text{km}, \tag{13}$$

where b_0 in kHz is the halfwidth of a high Q resonance centered at f_0, and $c/4\pi = 23.86$ for the units chosen. The vacuum value b_0 was found nearly a constant (≈ 105 kHz) for the TEM_{00q} modes between 54 and 66 GHz; thus the effective path length L_E is about 0.24 km. Losses due to coupling, conduction on the mirror surfaces, and diffraction ("spillover" at the spherical mirror) determine the value for b_0. Spurious fields inside the chamber, which might be excited by stray radiation, were suppressed with absorber material positioned off the resonance field. In rare cases, coincidence with a higher-order mode was suspected to be the cause of erroneous (b_x increased markedly over typical values) spectrometer readings.

3.2 Properties of the Resonance Signal

An automatic network analyzer (ANA, HP 85106A) was used, capable of making vector (magnitude and phase) measurements of a reflected signal with unprecedented speed, accuracy, and convenience. Between 10 and 15 GHz, the ANA's synthesized source generator (spectral purity and stability equal that of the internal 10 MHz quartz time base) provides a stimulus for the spectrometer resonator. A multiplier (× 5) transforms the RF signal to the 50 to 75 GHz band where the frequency resolution is typically 10 Hz. The RF signal changes frequency in discrete steps over a band Δf, centered at f_x and covering several halfwidths b. Reflected and incident signals from the resonator port are separately detected and their ratio is measured as complex reflection scattering coefficient,

$$s_{11}(\Delta f) = \mathbf{A}_c + \mathbf{A}_R(f). \tag{14}$$

The reflected signal amplitude and phase without a resonance is $\mathbf{A}_o = a' + ja''$, and $\mathbf{A}_R(f)$ is the frequency response of a high Q resonance. The ANA system allows calibration of the maximum reflection level to a normalized response, $a' = -1$ and $a'' = 0$.

The properties of an isolated resonance centered at f_x can be expressed by three interrelated (loaded = **Q**, unloaded = Q^o, and coupling = Q_c) Q values,

$$1/\mathbf{Q} = 1/Q^o + 1/Q_c.$$

For weak coupling and high Q values ($Q_c > \mathbf{Q} > 10^5$), the reflected signal is then given by a Lorentzian (Schulten, 1966) in the form

$$\mathbf{A}_R(f) = (1 - \mathbf{Q}/Q_o)/[1 + j2\mathbf{Q}(f - f_x)/f_x]; \quad (15a)$$

which, when one sets $a_x = 1 - \mathbf{Q}/Q^o$ and $b_x = f_x/2\mathbf{Q}$, changes to

$$\mathbf{A}_R(f) = a_x/[1 + j(f - f_x)/b_x]. \quad (15b)$$

The frequency position of the reflection minimum (amplitude dip) a_x defines f_x, while $\pm b_x$ sets the frequency extensions from f_x to where the amplitude dip has dropped to $1/\sqrt{2}$ its original value (power halfwidth).

A statistical analysis of $s_{11}(\Delta f)$ data with the method of least squares provided the general approach to extracting five parameters (a', a'', f_x, and Q_o, $\mathbf{Q}$ or a_x, b_x) from (15a or b). Pairs of unloaded and loaded Q values and of parameters a_x and b_x are both strongly coupled (correlation coefficient $\rho > 0.9$; i.e., random signal variations that widen b_x simultaneously increase a_x). Hence, an alternate functional form,

$$\mathbf{A}_R(f) = 1/[g_x + j(f - f_x)/S_R], \quad (16)$$

was introduced for $\mathbf{A}_R$ in (14). Here we substituted $(1 - \mathbf{Q}/Q^o) = \mathbf{Q}/Q_c$, and defined $g_x = Q_c/\mathbf{Q} = 1/a_x$ as an amplitude factor, and $S_R = f_x/2Q_c = a_x b_x$ as resonance strength. The parameters g_x and S_R were found to be nearly independent (correlation coefficient $\rho < 0.35$), making (16) a better choice for the nonlinear least squares fit that extracts a', a'', S_R, g_x, and f_x.

3.3 Measurement Principle and Test Gases

The parameters in (15) and (16), which are subscripted by x, change with pressure, whereby $x \equiv 0$ implies $P = 0$, the reference state, and x the air-filled state for a constant pressure P. A difference measurement is conducted between the reference and a filled state. When air is introduced into the evacuated chamber, simultaneous changes in the resonance shape ($a_0 \rightarrow a_x$ and $b_0 \rightarrow b_x$), and shifts in the center frequency ($f_0 \rightarrow f_x$), are translated into attenuation rates α (Sect. 3.4) and refractivities N' (Sect. 3.5) (Newell and Baird, 1965; Poon, 1977; Read et al., 1988).

Gas pressure P was stepped between 0 and 101 kPa, controlled by a piezo-electric leak valve. The temperature T_c of the insulated spectrometer cell was kept stable to ± 0.01°C. Pressure was changed slowly ($\leq \pm$ 10 kPa/min) to ensure quasi-static gas conditions. The vacuum $P = 0$ (2×10^{-5} kPa) was established with a two-stage rotary vane pump (750 l/min) followed by a zeolith sorption trap.

The test gases were laboratory-grade dry air (composition and impurities stated by the supplier: 79.3 percent N_2, 20.7 ± 0.21 percent $\mathbf{O}_2$, 2.1 ppm H_2O, ≤ 1 ppm CO_2, ≤ 0.1 ppm total hydrocarbon content) and nitrogen serving as a lossless ($\alpha = 0$) substitute for air.

3.4 Attenuation Measurement

The attenuation rate α can be computed from detected changes in the reflected, linearly-detected resonance signal. The parameters that are deduced from (15) allow one to formulate (L_E in km, b_0 in kHz)

$$\alpha_a = (4.343/L_E)\,[(a_0/a_x) - 1] = 0.1820 \cdot b_0\,[(a_0/a_x) - 1] \quad \text{dB/km}, \tag{17}$$

$$\alpha_b = (4.343/L_E)\,[(b_x/b_0) - 1] = 0.1820(b_x - b_0), \tag{18}$$

$$\alpha_{ab} = (\alpha_a + \alpha_b)/2. \tag{19}$$

A strong correlation between a_x and b_x suggest here to take (19) as an improved result. With the resonance parameters S_R and g_x of (16), attenuation is computed by (S_R in kHz)

$$\alpha_x = 0.1820 \cdot S_R(g_x - g_0). \tag{20}$$

Equations (17)-(20) are valid when the assumption $\alpha \cdot d_R << 4.3 \times 10^6$ holds (Read et al., 1988). In our case, $\alpha \cdot d_R \leq 4 \times 10^3$ since $\alpha \leq 20$ dB/km and $d_R \approx 200$ mm.

A measurement precision of ± 0.02 dB/km was the set goal for detecting attenuation. Meeting this goal with an effective path length of 0.24 km, requires that relative ratio changes of a_0/a_x and b_x/b_0 in (17) and (18) are detected to the order of 1×10^{-3}; or in terms of frequency differences, that about 100 Hz are resolved for the term $S_R(g_x - g_0)$ in (20).

3.5 Refractivity Measurement

The real part of the complex refractivity N(f) of a gas is measured simply by (Newell and Baird, 1965)

$$N_x = (f_0 - f_x)10^6/f_0 \quad \text{ppm}, \tag{21}$$

A measurement precision of 0.005 ppm is obtained at 60 GHz when the difference $f_0 - f_x$ is resolved to better than 300 Hz. The experimental value is the sum of three contributions,

$$N_x = N_s + N'(f) + N_c, \tag{22}$$

where N_s is nondispersive, $N'(f)$ is the dispersive refraction of the $\mathbf{O}_2$ microwave spectrum in air, and N_c is an instrumental correction term accounting for the drift of f_0. Dispersive contributions N_f are small (≤ 1 ppm, see Fig. 1) and nondispersive refractivity (3) reduces (independent of pressure and temperature) to a constant

$$R_s = 792.06 \cdot r_G = (N_x - N_c - N')(T/P) \quad \text{ppm·K/kPa}. \tag{23}$$

3.6 Computer Software for Spectrometer Operation

In order to best apply the ANA, new measurement procedures had to be developed. All spectrometer operations were controlled by a microcomputer. A comprehensive software package with 4,600 program lines was developed. The program offers various menus for single and multiple resonance scanning. Various subroutines

a) allow one to execute differing measurement configurations

b) set the operational parameters of ANA

c) control the pressure steps ΔP

d) control the data acquisition via a General Purpose Interface Bus (GPIB) from the following instruments:
- ANA
- Capacitance manometer (P)
- Precision quartz thermometer (T_c)
- Four-channel, fast response (τ = 0.5 s), scanning thermometer
  (one thermistor sensor is embedded in the resonator structure, three are sensing the open space)

e) initiate the automatic ("response") calibration to normalize the reflected signal level
(A_o, = - 1 + *j*0)

f) center the detected resonance signal at f_x and, as an option, adjust the stepped frequency span (Δf) with respect to the changing halfwidth b_x (see Sect. 4.1)

g) call the NLS (nonlinear least-squares) fitting routines, which reduce with the help of either (15) or (16) the s_{11} data sets to the desired resonance parameters.

4. EXPERIMENTAL PROCEDURE

4.1 Single Resonance Detection

A first step in the detection process was the normalization of the off-resonance signal level s_{11} to A_o = - 1 + *j*0 over the frequency span Δf. A "response" calibration (ANA feature) with a short provided the reference. The waveguide plane of the coupling iris acts as short when, under computer control, the resonance is defeated (**A** = 0) with a motor-driven metal vane that rotates into the resonance space.

Optimization of the detection of s_{11} data at a resonance f_x was an important objective. A feature of the ANA is the superheterodyne detection scheme with an intermediate frequency (IF) of 20 MHz. A synthesized generator (identical to the RF source) serves as local oscillator (LO) for the harmonic (× 14) mixers that detect reflected and incident signals. Both IF signals are amplified, down-converted to 100 kHz, then detected and processed. The output is a normalized signal ratio called reflection scattering (S) parameter $s_{11}(f)$. The S-parameter is sampled in even increments over the span Δf at a number (pts) of fixed frequency points each being averaged a number (avg) of times. An example of an S-parameter set is listed in Table 2, and the equivalent in log magnitude (power dB) and phase angle (deg) is plotted in Figure 5. The influence of various combinations by the three variables "Δf", "pts", and "avg" upon s_{11} was studied in detail.

- The frequency span was set at $\Delta f = 5 \cdot b_x$, centered at f_x to cover the amplitude range of a resonance response to about $a_x/9$. Centering at f_x was done automatically. Initially, the span Δf followed the changes of the halfwidth, $b_x(\alpha) - b_0$ ($\leq$ 90 kHz). However, this required an additional calibration adding about 10 seconds to each run. A comparison of both methods yielded identical results, (17) to (21). To not slow down the many production runs, a constant value Δf = 500 kHz was kept.

- For stepped frequency points, the choice is 51, 101, 201, 401 or 801 pts. Frequency switching time is about 50 msec.

- Averaging (avg) is possible in powers of 2^y (y = 1 to 12) at a speed of 5,000 values per second.

The optimum combination "Δf-pts-avg" is constrained by three factors: achievable frequency resolution ($\leq$ 100 Hz for both resonance center f_x and width b_x), inherent noise level ($\delta s_{11}/s_{11} \leq 0.0003$), and desired acquisition time ($t_x \leq 5$ s). After extensive test series (see Sect. 4.3), the reflected signal was measured around f_x by stepping in 10 kHz increments (51 pts) over a scan range of 500 kHz (Δf), averaging each point 128 (avg) times, in a total acquisition time of 2 seconds (t_x). Subsequent processing of s_{11} data used formulas (17) to (21), whereby the relevant parameters were deduced by fitting data strings of s_{11} to the analytical function given by either (15) or (16). A fast, nonlinear least-squares (NLS) routine was developed by us that worked very well. The method was based on the iterative Levenberg-Marquardt algorithm (Marquardt, 1963), which has become the standard of NLS routines. Two different sets of output parameters could be generated.

1) The NLS.1 fit to (15) produced center frequency, f_x, loaded and unloaded Q values, **Q** and Q^o, the reference signal level, a′, a″, and the standard fitting error of each parameter.

2) The NLS.2 fit to (16) replaced the two Q-values of NSL-1 with S_R and g_x. In addition, real and imaginary parts of the individual residuals $\delta s_{11}(\Delta t)$ were provided; also their rms standard deviations, σ_s, and the three correlation coefficients, $\rho_1(f_0 \rightarrow g_0)$, $\rho_2(f_0 \rightarrow S_R)$, and $\rho_3(g_0 \rightarrow S_R)$.

Several multi-parameter NLS fitting schemes were tested and the three accepted ones are summarized in Table 3. The F3 scheme initially infers five parameters, which serve as input for the final fit to the two parameters that determine α and N′. That scheme proved most useful and was applied to the production runs.

4.2 Multiple Resonance Operation

The resonator supports a comb of resonances, which were computed with (12). The computer tunes to multiple $TEM_{0,0,q}$ resonances (e.g., q = 79 to 88), which appear in c/2L-intervals (e.g., 0.7330 GHz for d_R = 204.5 mm) with loaded Q-factors, $\mathbf{Q}_0 \approx 2.5$ to 3.5×10^5. Multiple resonances can be utilized for one P-T combination as long as the coupling yields a sufficient signal level. For a tolerable signal-to-noise ratio, the needed amplitude a_0 was $\geq 0.01a'$. On the other hand, for a symmetric resonance response and a high **Q** factor, adequate decoupling ($\leq 0.1a'$) had to be ensured.

Example of Real and Imaginary Parts of the ANA Signal s_{11}
(101pts/256avg; 62.48 GHz, 101 kPa air, 30°C)

f	*Re*	*Im*	f	*Re*	*Im*	
62482835615.	-.99332	.01453	62483243615.	-.96036	.00076	
62482843615.	-.99420	.01413	62483245266.	-.96074	.00000	f_x
62482851615.	-.99332	.01477	62483251615.	-.96014	-.00092	
62482859615.	-.99310	.01468	62483259615.	-.96054	-.00284	
62482867615.	-.99277	.01489	62483267615.	-.96082	-.00473	
62482875615.	-.99234	.01477	62483275615.	-.96143	-.00668	
62482883615.	-.99200	.01508	62483283615.	-.96228	-.00818	
62482891615.	-.99188	.01532	62483291615.	-.96304	-.00977	
62482899615.	-.99146	.01575	62483299615.	-.96362	-.01132	
62482907615.	-.99164	.01584	62483307615.	-.96500	-.01254	
62482915615.	-.99081	.01611	62483315615.	-.96588	-.01370	
62482923615.	-.99054	.01627	62483323615.	-.96735	-.01492	
62482931615.	-.99036	.01620	62483331615.	-.96848	-.01590	
62482939615.	-.99005	.01639	62483339615.	-.96997	-.01672	
62482947615.	-.98975	.01691	62483347615.	-.97083	-.01730	
62482955615.	-.98917	.01721	62483355615.	-.97235	-.01785	
62482963615.	-.98871	.01749	62483363615.	-.97342	-.01804	
62482971615.	-.98853	.01755	62483371615.	-.97452	-.01886	
62482979615.	-.98792	.01773	62483379615.	-.97580	-.01901	
62482987615.	-.98746	.01794	62483387615.	-.97675	-.01923	
62482995615.	-.98746	.01819	62483395615.	-.97781	-.01917	
62483003615.	-.98651	.01871	62483403615.	-.97885	-.01923	
62483011615.	-.98615	.01880	62483411615.	-.97980	-.01944	
62483019615.	-.98532	.01862	62483419615.	-.98077	-.01929	
62483027615.	-.98471	.01889	62483427615.	-.98166	-.01929	
62483035615.	-.98392	.01907	62483435615.	-.98257	-.01907	
62483043615.	-.98312	.01926	62483443615.	-.98343	-.01917	
62483051615.	-.98251	.01953	62483451615.	-.98419	-.01892	
62483059615.	-.98175	.01938	62483459615.	-.98486	-.01877	
62483067615.	-.98071	.01959	62483467615.	-.98547	-.01865	
62483075615.	-.97974	.01968	62483475615.	-.98599	-.01831	
62483083615.	-.97913	.01987	62483483615.	-.98669	-.01813	
62483091615.	-.97787	.01944	62483491615.	-.98737	-.01813	
62483099615.	-.97696	.01929	62483499615.	-.98776	-.01755	
62483107615.	-.97629	.01907	62483507615.	-.98834	-.01718	
62483115615.	-.97482	.01892	62483515615.	-.98920	-.01703	
62483123615.	-.97382	.01874	62483523615.	-.98935	-.01712	
62483131615.	-.97256	.01837	62483531615.	-.98972	-.01660	
62483139615.	-.97134	.01791	62483539615.	-.99011	-.01645	
62483147615.	-.97031	.01730	62483547615.	-.99081	-.01596	
62483155615.	-.96921	.01627	62483555615.	-.99121	-.01578	
62483163615.	-.96814	.01544	62483563615.	-.99152	-.01572	
62483171615.	-.96640	.01453	62483571615.	-.99161	-.01553	
62483179615.	-.96548	.01315	62483579615.	-.99197	-.01517	
62483187615.	-.96463	.01236	62483587615.	-.99207	-.01517	
62483195615.	-.96338	.01105	62483595615.	-.99246	-.01471	
62483203615.	-.96252	.00919	62483603615.	-.99289	-.01440	
62483211615.	-.96179	.00787	62483611615.	-.99301	-.01398	
62483219615.	-.96106	.00613	62483619615.	-.99341	-.01419	
62483227615.	-.96072	.00400	62483627615.	-.99301	-.01416	
62483235615.	-.95993	.00247	62483635615.	-.99368	-.01398	

Table 3

NLS Fitting Schemes to s_{11} (Levenberg-Marquardt method)

Code	Eqn	Para.	Level Cal.	Resonance Properties			Repeats × s_{11}	Repeats × P
F1	(15)	5	a′,a″	Q°	Q	f_x	1	1
F2	(15)	5	a′,a″	Q°	Q	f_x	10	1
F3	(16)	5+2	a′,a″	S_R	g_x^i	f_x^i	10	11
		-	-	-	g_x	f_x	10	1

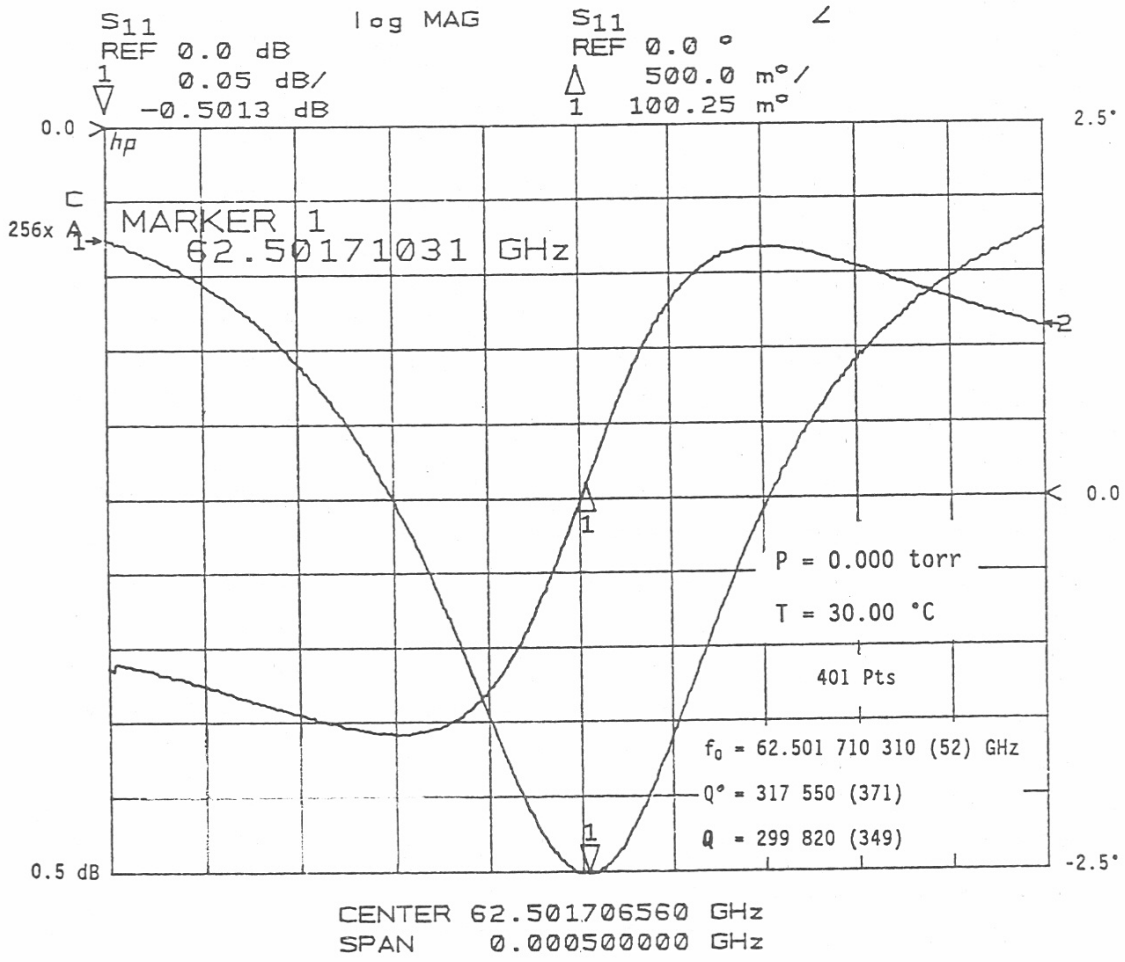

Figure 5. Typical reflected resonance signal s_{11}, as displayed by ANA in log magnitude (power dB) and phase angle (deg) (f_0, Q and Q° from an F1 fit).

The diameter of the coupling iris in combination with an adjustable coupling circuit determines the usable frequency range. Two flat mirrors with different coupling irises (1.0 and 1.1 mm diameter) were available. The first produced adequate coupling down to 58 GHz, while the larger iris excited resonances as low as 49 GHz. A resonant (Q-value, **Q** ≈ 20) coupling circuit is made up by the surface, which retains the iris, followed by a cylindrical cavity (8 mm dia.) of adjustable length, l_c = 0.1 to 8 mm, and a quartz glass window (6.4 dia. × 0.64 mm) that provides the vacuum seal.

For the example exhibited in Figure 6, a maximum coupling of $a_0 \approx 0.08$ was adjusted at 61.5 GHz with $l_c \approx 3$ mm. Ten resonances were excited whereby the peak signal dropped over a span of ± 3.5 GHz to $a_0 \approx 0.01$. The amount of coupling to some extent affected the symmetry of a resonance. The quality of recorded s_{11} data improved when the measurements were organized in three groups of five resonances. This allowed a total of thirteen f_x (the 5th and 6th being the same, and also the 10th and 11th) to cover the range from 58 to 67 GHz. In this case, the coupling was adjusted (l_c) to yield amplitudes $a_0(f_0)$ between 0.08 and 0.02 with symmetric $s_{11}(\Delta f)$ data.

At the selected resonance frequencies f_x, each measurement sequence was repeated ten times before increasing the pressure. In addition to the initial and final record at P = 0 (reference state), ten pressure values were preprogrammed. The data acquisition was fully automated. A typical run with five sequential resonances took about one hour.

4.3 Sensitivity and Longterm Stability

The challenge of operating a spectrometer in the 60 GHz range lies in recovering small frequency differences (≤ 100 Hz) from the envelope response of two resonance states [see (20),(21)]. The ANA supplies a fixed power RF signal at specified frequencies, and the calibrated response is measured with little error for amplitude (dynamic gain) and phase (frequency) instabilities. The s_{11} parameters are detected with a precision equal to 3×10^{-5} (16-bit A/D converter, including sign) at a noise level, $ds_{11} \approx 3 \times 10^{-4}$, which is an analytical estimate that was obtained by comparing rms values of residuals from NLS fits (seeSect. 5.2).

Results of test runs under different detection conditions (varied values of pts and avg) are listed in Table 4. They were evaluated (F1) for resolutions in center frequency (δf_0) and in loaded Q-value ($\delta \mathbf{Q}_0$). The number of frequency steps (pts) determines the resolution of f_x. The error in fitting **Q** is reduced as either "pts" or "avg" increase, being more sensitive to "pts". Averaging only 128 times appeared reasonable since doubling the number reduces the errors by only a few percent. Note, that as "pts" is increased, the residuals of a fit grow smaller and the fluctuations of the longterm (500 ×) time series intensify, as indicated by their rms standard deviation, σ_Q. More "pts" require a longer time interval t_x for a scan. During this interval, the resonance changes its shape due to ANA phase drifts.

Another performance evaluation involved 24-hour repeat runs to check on the long term stability of $\alpha = 0$ for different combinations of pts/avg. Test data were taken repeatedly under vacuum conditions for various system configurations to determine stability and accuracy of the detection method. Reflection data were

Table 4

F1-Fitting Errors δf, δQ, and Standard Deviations, σ_Q, of Repeat (500×) Runs for a Single Resonance ($P = 0$, $f_x = 62.5$ GHz, $Q \approx 3\times10^5$, $a_x = 0.062$)

Number of Points	Averages	Duration t_x	Standard Error from NSL-fit δf_x	δQ	σ_Q
pts	avg	sec	Hz		
51	**128**	2	232	1900	735
	256	4	225(10)	1505(66)	655
	512	8	214		
	1024	12	218(20)	1466(130)	1150
101	**256**	8.5	149(11)	**1006**	**1050**
	512	17	133		
201	64	4		1000	946
	128	8.5	112		
	256	17	105(8)	710(57)	1340
	512	33	108		
401	128	17	96		
	256	33	75(7)	513(52)	3110
	512	70	72		

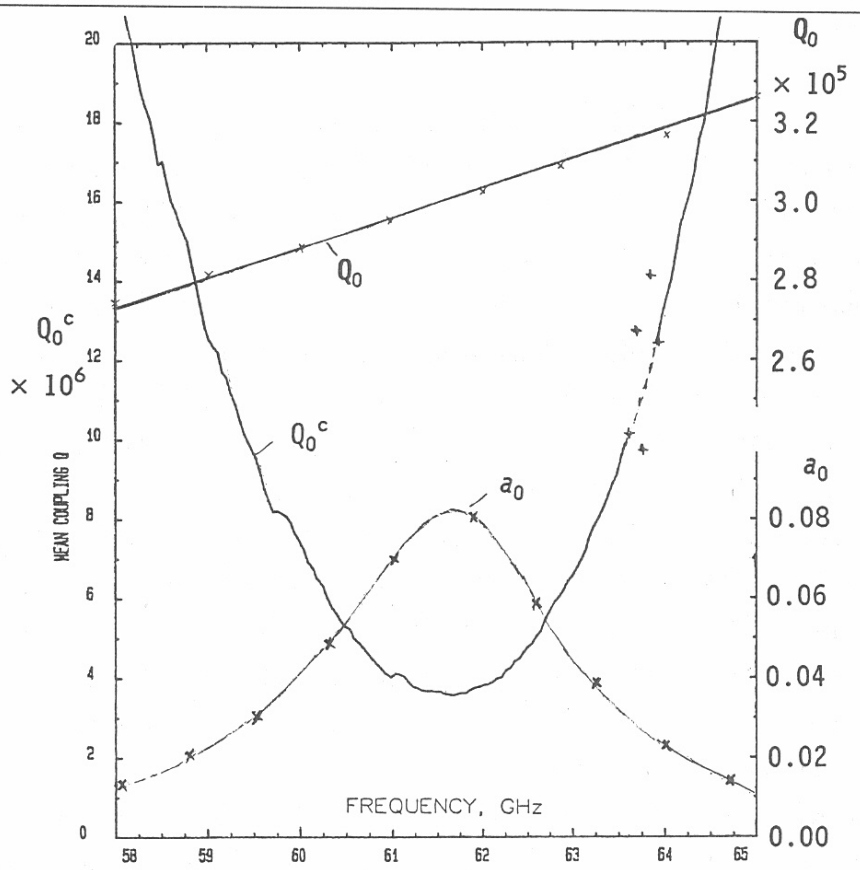

Figure 6. Measured Q values (Q - loaded, Q_c - coupling) and resonance amplitudes a_0 from 58 to 65 GHz for $d_R = 204.5$ and $l_c \approx 3$ mm at $P = 0$ and $T = 30°C$.

analyzed on-line by repeatedly applying F1 (500 ×) over 24-hour periods. Individual acquisition times and rms standard deviations from the mean, $\alpha = 0$, of the time series are listed in Table 5. The 51/128-case indicates that a fast scan produces s_{11} data of acceptable quality (see Fig. 4). Baseline variability for α_{ab} is about the same as for α_a; for longer time periods, the correlation between α_a and α_b improves the average.

Table 5

Longterm Detection Characteristics At 62.5 GHz
(see Fig. 7)

Pts	Avg	t_x	σ_a (17)	σ_b (18)	σ_{ab} (19)
		s		dB/km	
51	**128**	2.1	0.025	0.047	0.029
201	64	4.2	0.026	0.060	0.028
101	256	8.4	0.036	0.066	0.026

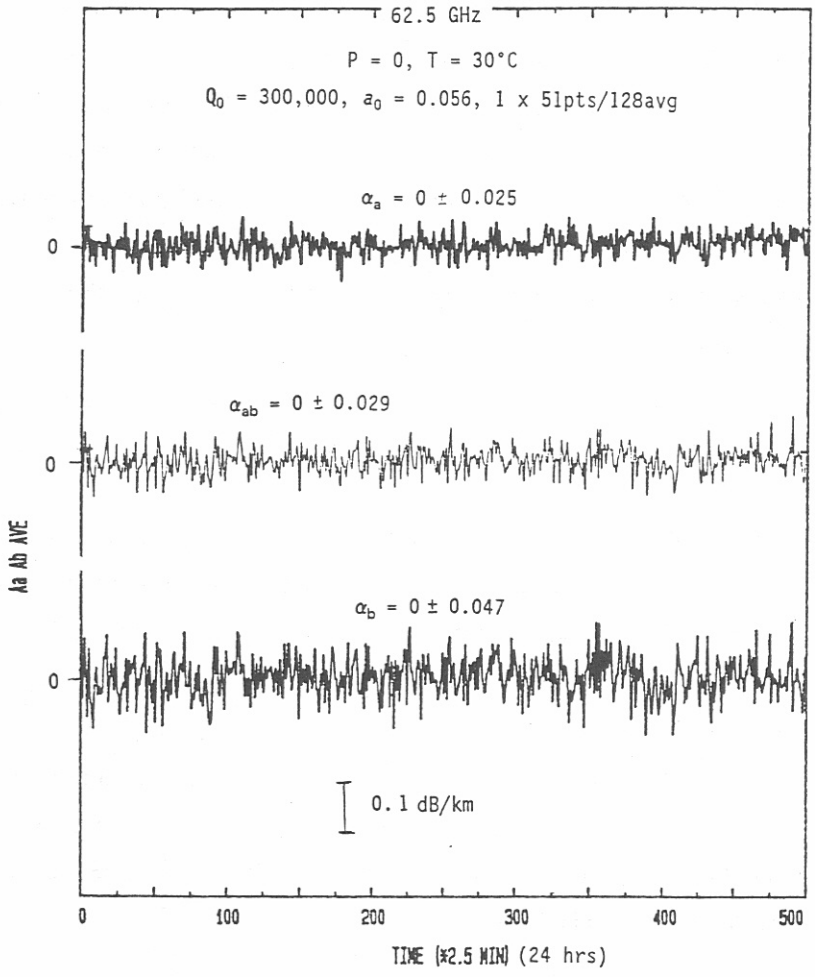

Figure 7. Longterm (24 hrs) behavior at 62.5 GHz for a repeat run (500x).